

Principal Sub-manifolds

October 11, 2024

Zhigang Yao
 Department of Statistics and Applied Probability
 21 Lower Kent Ridge Road
 National University of Singapore, Singapore 117546
 email: zhigang.yao@nus.edu.sg

Tung Pham
 School of Mathematics and Statistics
 University of Melbourne
 Victoria 3010 Australia
 email: pham.t@unimelb.edu.au

Abstract

We revisit the problem of finding principal components to the multivariate datasets, that lie on an embedded nonlinear Riemannian manifold within the higher-dimensional space. Our aim is to extend the geometric interpretation of PCA, while being able to capture the non-geodesic form of variation in the data. We introduce the concept of a principal sub-manifold, a manifold passing through the center of the data, and at any point on the manifold, it moves in the direction of the highest curvature in the space spanned by eigenvectors of the local tangent space PCA. Compared to the recent work in the case where the sub-manifold is of dimension one [19]—essentially a curve lying on the manifold attempting to capture the one-dimensional variation—the current setting is much more general. The principal sub-manifold is therefore an extension of the principal flow, accommodating to capture the higher dimensional variation in the data. We show the principal sub-manifold yields the usual principal components in Euclidean space. By means of examples, we illustrate how to find, use and interpret principal sub-manifold with an extension of using it in shape analysis.

Keywords: manifold, principal component analysis, tangent space, dimension reduction, shape analysis

1 Introduction

Not all data are Euclidean or linear. Manifold data arises in the sense that the sample space of data is fundamentally nonlinear. Among them, there are data that can be seen as lying on spheres dating back as early as [4] in directional statistics, or more generally, as lying on Riemannian manifolds in shape deformation. The latter in particular has posed

an interesting question to study the linkage between the data space, e.g., configurations of landmarks representing a population, and the *induced* curved shape space. The aim is to make useful statistical inference with respect to the underlying manifold space suggested by the data. To accomplish this goal, a basic step is to transfer the usual coordinate system of the data to a new one indicating its position on the manifold. This can be done either by transforming it to a so-called “known manifold” [16] or by learning an “unknown manifold.” In this paper, we will mainly focus on the known manifold scenario. This kind of problem becomes increasingly important, as many procedures in medical imaging [2, 8] and computer vision produce data [20, 21] in such forms. The differences are that although one can view each observation such as an image as a point in a high-dimensional space, it is more likely to represent a collection of such images using a lower dimensional nonlinear manifold. In a real application, working with the manifold space can help reduce the uncertainty, as it provides more reasonable distance metrics. However, the methodology built directly upon manifold space is still underdeveloped. The primary reason is that conventional statistical methodology based on vector space is not so adaptive when it comes to manifold space. The simplest case is that the notation of sample mean on manifold does not guarantee the existence and uniqueness anymore [7]. To quantify statistical variation on more complex features such as curves and surface, a strategy of developing statistical tools in parallel with their Euclidean-counterpart is significantly relevant.

There have been a number of studies on manifold space over the past decades, most of which try to find the center and the main modes of variation in the data, provided with a curved metric. Roughly speaking, one first expects to find reasonable means of the data (called Fréchet means) and standard deviations, and then find a certain sub-manifold almost explaining the variability of data. Though we have witnessed an increasing effort in developing statistical approaches based on nonlinear manifolds, seemingly from various perspectives, the major effort has been focused on extending the principal component analysis (PCA) to a manifold version. Equipped with Riemannian metrics on shape space, principal geodesics [6, 11, 10, 17, 13] is a manifold version of PCA by replacing the straight lines in Euclidean space with its geodesic analogue on manifolds. Geodesic fitting approaches try to define smooth curves directly in shape space, with reference to the *preshape* space. Using more general spline functions of a certain type on manifolds [15] and [18] developing smooth curves by unrolling and unwrapping the shape space primarily involves transportation of the target curve between the manifold and the tangent space at the starting point—usually sequentially indexed. By finding a sequence of nested linear sub-manifolds (essentially spheres, [13]) with decreasing dimensionality, the principal nested spheres decompose the sample space locally near the mean by sequentially “fitting” within each dimension such that these linear subspaces maximize the variance of the projected data [6]. Tangent space PCA [5] attempts to project the manifold data by simply lifting them to the relevant tangent space, and approximate the data distribution locally at the lifting point on the manifold with the induced Euclidean space. The use of tangent space on one hand makes manifolds much easier to work with, as it allows for tractable statistics; on the other hand, this generalization of PCA is conservative in the sense that the results are more guaranteed when the data clouds are concentrated. By retaining the classical PCA interpretation at each point of the curve, the principal flow [19] is a recently developed approach. Defined upon the manifold, the flow attempts to follow the main direction of the data cloud locally, nevertheless being able to accommodate the “curve fitting” characteristic on the manifold, and therefore admits a global property.

We consider generalizations for principal flow. The idea is to generalize the flow to a

surface or more generally a sub-manifold. The heuristic is the following: if one expects the majority of a data cloud to follow roughly a sub-manifold with an intrinsic dimension more than one, then it is crucial to describe the space of all possible sub-manifolds. In finding such a sub-manifold, we start from the center of the data cloud or any other point of symmetry on the manifold, just like the principal flow; but unlike the principal flow that moves along the maximum direction of variation of the data, we let the sub-manifold expand in all directions simultaneously. In principle, the sub-manifold is not supposed to move equally in any direction. Rather, it is expected to move around guided by the eigenvectors of the local covariance matrix. To form such a sub-manifold with an appropriate expansion, the curvature plays an essential role.

However, identifying a potentially better sub-manifold out of all the possible ones can be non-trivial. It is essentially an optimization problem that consists of comparing one surface with another, subjected to some smooth conditions. The same problem has appeared in finding the principal flow. With this being said, parameterizing curves is much easier than parameterizing surfaces as the latter requires integration along the surface. We introduce two definitions of the principal sub-manifold; the first definition is a conceptual one that does not rely on the actual parameterization of the surface, and the second definition involves a specific parameterization of the surface, and therefore is a concrete one. Although both definitions seem sound, the algorithm of finding the principal sub-manifold is given based on the second definition.

We formally define the principal sub-manifold (Section 2.4) as a sub-manifold in which at any point of the sub-manifold, the hyperplane of the sub-manifold attempts to be close to that of the data manifold; intuitively, this definition is an analogue to the definition of the principal flow. We show that in case of flat space, the principal sub-manifold reduces to the space spanned by principal components, in which the dimension of the sub-manifold corresponds to the number of principal components. Theorem 1 is proved in Section 6. The principal sub-manifold also provides a complementary notation to that of a principal surface by [9], as a self-consistent surface defined in Euclidean space.

The remaining part of the paper is organized as follows. We start with an overview of the principal flow with some necessary background on Riemannian geometry and statistical shape analysis (Section 2.1-2.3). In Section 3, we first investigate an algorithm for determining the principal sub-manifold; then we describe the representation of the principal sub-manifold, with a special example of visualizing a two-dimensional sub-manifold for data in $S^3 \subset \mathbb{R}^4$. Section 4 contains examples; we illustrate by means of simulated examples and the analysis of leaf growth data and handwritten data that the principal sub-manifold is capable of representing more general aspects of data variation compared to the principal flow. We end this paper with a discussion.

2 Principal Sub-manifolds

2.1 Preliminaries

Suppose that $\{x_1, \dots, x_n\}$ are n data points on a complete Riemannian manifold (\mathcal{M}, g) of dimension m , embedded in the linear space \mathbb{R}^d , where $m < d$. Here, g is a Riemannian metric defined on the manifold \mathcal{M} . To be specific, let any point x to be on the tangent space $T_x \mathcal{M}$, then g is a smooth family of inner products:

$$g_x : T_x \mathcal{M} \times T_x \mathcal{M} \rightarrow \mathbb{R}.$$

Given any x , the inner product induces a norm on $T_x\mathcal{M}$, that is, for every $v \in T_x\mathcal{M}$, the norm of v is denoted by

$$\|v\| = \sqrt{g_x(v, v)}.$$

For simplicity, we will only refer \mathcal{M} as a Riemannian manifold where the metric is implicit. See [3] for a quick review of manifold.

Throughout this paper, we assume that the embedding is explicitly known, that is, there always exists a differentiable function $F : \mathbb{R}^d \rightarrow \mathbb{R}^m$. Thus, the manifold \mathcal{M} is the set such that

$$\mathcal{M} := \left\{ x \in \mathbb{R}^d : F(x) = 0 \right\}.$$

For each $x \in \mathcal{M}$, the tangent space at x will be denoted by

$$T_x\mathcal{M} := \left\{ y : DF y = 0, y \in \mathbb{R}^d \right\}$$

with the induced Riemannian metric and metric tensor. Here, DF is $m \times d$ derivative matrix of F evaluated at $x \in \mathcal{M}$, assumed to be of full rank everywhere on \mathcal{M} . Thus, $T_x\mathcal{M}$ is in fact a *vector space*, the set of all tangent vectors to \mathcal{M} at x , which essentially provides a local vector space approximation of the manifold \mathcal{M} . This is by analogue the derivative of a real-valued function that provides a local approximation of the function.

Definition 2.1 *A curve, $\gamma : [0, 1] \rightarrow \mathcal{M}$ is a geodesic if and only if $\dot{\gamma}(t)$ is parallel along γ , that is, the acceleration vector*

$$\frac{d(\dot{\gamma})}{dt} = 0.$$

This means that $\frac{d(\dot{\gamma})}{dt}$ is normal to $T_{\gamma(t)}\mathcal{M}$ at any time t .

By equipping the manifold with the tangent space, we define mappings back and forth between $T_x\mathcal{M}$ and \mathcal{M} . There are two kinds of mappings of interest: 1) the exponential map¹, being well defined in terms of geodesics, is the map,

$$\exp_x : T_x\mathcal{M} \rightarrow \mathcal{M} \tag{2.1}$$

by $\exp_x(v) = \gamma_v(1)$ meaning that $\exp_x(v)$ is obtained by following the geodesic starting from $\gamma(0) = x$ with initial velocity $\dot{\gamma}(0) = v$ for 1 unit, and 2) the logarithm map (the inverse of exponential map), is locally defined at least in the neighborhood of $\exp_x(v)$ of x ,

$$\log_x : \mathcal{M} \rightarrow T_x\mathcal{M}. \tag{2.2}$$

Let p and q be in \mathcal{M} . Denote all (piecewise) smooth curves $\gamma(t) : [0, 1] \rightarrow \mathcal{M}$ with endpoints such that $\gamma(0) = p$ and $\gamma(1) = q$. The *geodesic distance* from p to q is defined as

$$d_{\mathcal{M}}(p, q) = \inf \ell(\gamma) \tag{2.3}$$

where $\ell(\gamma) = \int_{[0,1]} \|\dot{\gamma}(t)\| dt = \int_{[0,1]} g_{\gamma(t)}(\dot{\gamma}(t), \dot{\gamma}(t))^{\frac{1}{2}} dt$. Minimizing (2.3) yields geodesics as in Definition 2.1, the shortest distance between two points p and q in \mathcal{M} .

Definition 2.2 *The Fréchet mean, \bar{x} , for a sample of data points $\{x_1, \dots, x_n\} \in \mathcal{M}$ is a minimizer of the Fréchet variance*

$$\frac{1}{n} \sum_{i=1}^n g^2(p, x_i), \quad p \in \mathcal{M}$$

under the Riemannian metric g .

¹away from the cut locus of x on $T_x\mathcal{M}$

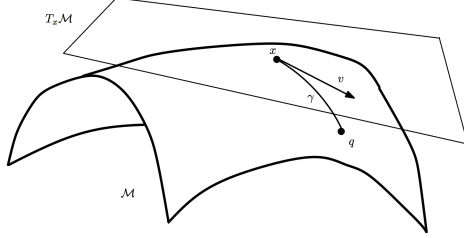


Figure 1: The subspace v on the tangent plane $T_x\mathcal{M}$ at x . The endpoint of vector v is the image of $q = \mathbf{exp}_x(v)$ under the mapping defined in (2.2).

2.2 Embedding of shape space for landmarks

In geometrical shape analysis, landmark coordinates retain the geometry of a certain point configuration. The landmarks are observations, which are usually positions or correspondences on an object in an appropriate coordinate axes. When considering a suitable ordered set of k landmarks of an object in \mathbb{R}^d (usually $d = 2$), namely a k -ad (where $k \geq 2$), with each one being

$$x = \left\{ x^j \in \mathbb{R}^d : 1 \leq j \leq k \right\},$$

one would like to know how a certain shape of an object out of a collection of several x 's differs from the other. As an object's shape should not change under translation, scaling or rotation, two objects with the same shape should line up exactly. Here, we briefly mention a shape matching representation called Kendall shape space (Σ_2^k), which is invariant under translation, scaling, and rotation. The following steps lead to transforming any k -ad, x , to a point on the unit sphere:

Translation: remove the effects of translation by $x^* = x - \bar{x}$, where $\bar{x} = \frac{1}{k} \sum_{j=1}^k x^j$

Normalization: remove the effect of scaling by $x_{\text{pre}} = \frac{x^*}{\|x^*\|}$

Rotation: $[x] = R(\theta)x_{\text{pre}} = e^{i\theta}x_{\text{pre}}$, where $-\pi < \theta \leq \pi$.

Remarks: when $d = 2$, the translated x^* lies in the hyperplane of \mathbb{R}^{2k-2} ; after translation and normalization, x_{pre} is called the *preshape* of x . The space of x_{pre} is identified as the unit sphere $S^{2k-3} \subset \mathbb{R}^{2k-2}$. Here “-2” comes from losing 2 degrees of freedom in the translation step, and “3” comes from the definition of unit sphere

$$S^k = \left\{ v \in \mathbb{R}^{k+1} : \|v\| = 1 \right\}. \quad (2.4)$$

The $[x]$ is the *shape* of x given by the *orbit* of the preshape x_{pre} under rotation. The Σ_2^k is a quotient space of S^{2k-3} with dimension $2k - 4$. This shape space is the equivalent classes of all such k -ads after removing the effects of translation, scaling and rotation.

2.3 Principal flows

Before introducing the principal sub-manifold, we recall the concept of the principal flow. In [19], a *principal flow* has been proposed to capture the non-geodesic variation of a given

set of data points $\{x_1, \dots, x_n\}$ lying on a manifold \mathcal{M} . The flow is a curve resting on the manifold passing through the center of the data points, and at any point on the flow, its tangential velocity attempts to be parallel with the maximal direction of variation of the data points at that point.

Here, we only briefly review the principal flow (see [19] for a full treatment) using a sub-manifold representation. It is chosen as a matter of convenience in later derivations and can be thought of as drawing a connection to the principal sub-manifold. As any flow on \mathcal{M} is a one dimensional sub-manifold of \mathcal{M} , we can parameterize the sub-manifold explicitly using unit speed parameterization such that

$$\text{SubM}(A, v, \mathcal{M}) = \left\{ \gamma : [0, r] \rightarrow \mathcal{M}, \gamma \in C^2(\mathcal{M}), \gamma(s) \neq \gamma(s') \text{ for } s \neq s', \right. \\ \left. \gamma(0) = A, \dot{\gamma}(0) = v, \ell(\gamma[0, t]) = t \text{ for all } 0 \leq t \leq r \leq 1 \right\}. \quad (2.5)$$

where $\gamma(0) = A$ and $\dot{\gamma}(0) = v$ are initial conditions for γ and $\ell(\gamma)$ is the length of γ . The starting point A can be chosen as the Fréchet mean \bar{x} or any other point of interest. This says that $\text{SubM}(A, v, \mathcal{M})$ contains all smooth curves with a given initial speed and starting point, as well as their length being all less than 1.

To find a curve from the potential curves set in (2.5), the principal flow is defined as a solution that involves two curves γ^+ and γ^- to the following variational problem

$$\gamma^+ = \arg \sup_{\gamma \in \text{SubM}(A, v_1, \mathcal{M})} \int_0^{\ell(\gamma)} \langle \dot{\gamma}(t), e_1(\gamma(t)) \rangle dt \quad (2.6)$$

$$\gamma^- = \arg \inf_{\gamma \in \text{SubM}(A, v_2, \mathcal{M})} \int_0^{\ell(\gamma)} \langle \dot{\gamma}(t), e_1(\gamma(t)) \rangle dt \quad (2.7)$$

where as in (2.5), $v_1 = e_1(A)$, $v_2 = -v_1$, $e_1(A)$ is the first eigenvector of the covariance matrix Σ_A at A . The integral for γ^- is negative, which explains why the infimum appears in its definition. At each point of γ , $\dot{\gamma}(t)$, is maximally compatible to the eigenvector of local PCA at the same point. Often, the local covariance matrix at scale h is used

$$\Sigma_{h,A} = \frac{1}{\sum_i \kappa_h(x_i, A)} \sum_{i=1}^n \log_A(x_i) \otimes \log_A(x_i) \kappa_h(x_i, A) \quad (2.8)$$

where $\kappa_h(x, A) = K(h^{-1} \|\log_A x - A\|)$.

The innovation of the principal flow is two-fold: to differentiate from principal geodesic curves, principal flow is not necessarily a geodesic on the manifold, which gives an opportunity to capture non-geodesic variation from the manifold data; to differentiate from other curve-fitting approaches, principal flows are data dependent and quite flexible in trading-off the local PCA and the curve fitting characteristic.

In [19], principal flows are proved that they reduce to the usual principal components in the context of Euclidean space when the local covariance matrix is replaced by the global covariance matrix ($h = \infty$). They are therefore the manifold counterpart of the principal curves [9]. We also note that the principal surfaces are the extension of the principal curves to higher dimensions in Euclidean space, restricted to a two-dimensional scenario.

Motivated by a desire of capturing more nonlinear variation in more dimensions, we extend the principal flow to a higher dimensional manifold. In this sense, the manifold is a

multi-dimensional version of the principal flow, which we will call a principal sub-manifold. The following work is connected to both principal flow and the principal surfaces, but the setting it entails are more general.

2.4 Principal sub-manifolds

As before, denote $\{x_1, \dots, x_n\}$ to be the data points on \mathcal{M} . We will give a definition of the multi-dimensional manifold \mathcal{N} of $\{x_1, \dots, x_n\}$, starting from a point of interest x on \mathcal{M} . The sub-manifold is denoted as \mathcal{N} , differentiating it from the manifold \mathcal{M} .

For any point x in \mathcal{M} and \mathcal{N} , define $\Sigma_{x,\mathcal{M}}$ and $\Sigma_{x,\mathcal{N}}$ as the two tangent covariance matrices

$$\begin{aligned}\Sigma_{x,\mathcal{M}} &= \frac{1}{n} \sum_{i=1}^n \mathbf{log}_{x,\mathcal{M}}(x_i) \otimes \mathbf{log}_{x,\mathcal{M}}(x_i) \text{ and} \\ \Sigma_{x,\mathcal{N}} &= \frac{1}{n} \sum_{i=1}^n \mathbf{log}_{x,\mathcal{N}}(x_i) \otimes \mathbf{log}_{x,\mathcal{N}}(x_i).\end{aligned}$$

Let $\{\lambda_1(x, \mathcal{M}), \dots, \lambda_k(x, \mathcal{M})\}$ and $\{e_1(x, \mathcal{M}), \dots, e_k(x, \mathcal{M})\}$ be the first k eigenvalues and eigenvectors of $\Sigma_{x,\mathcal{M}}$. Correspondingly, we have k eigenvalues $\{\lambda_1(x, \mathcal{N}), \dots, \lambda_k(x, \mathcal{N})\}$ and eigenvectors $\{e_1(x, \mathcal{N}), \dots, e_k(x, \mathcal{N})\}$ for $\Sigma_{x,\mathcal{N}}$. Let $H_k(x, \mathcal{M})$ be the hyperplane on \mathcal{M} spanned by $\{e_1(x, \mathcal{M}), \dots, e_k(x, \mathcal{M})\}$; $H_k(x, \mathcal{N})$ be the hyperplane on \mathcal{N} spanned by $\{e_1(x, \mathcal{N}), \dots, e_k(x, \mathcal{N})\}$.

The key insight of finding a one dimensional sub-manifold is that its curves are well parameterized and the integral along the curve is invariant under different parameterizations; the latter plays a key role in determining principal flow, but is unfortunately an obstacle for general sub-manifolds with dimensions more than one. For the higher dimensional sub-manifold, we will define the sub-manifold locally.

For any point p belonging to the sub-manifold \mathcal{N} , define

$$\mathbf{B}(x, \mathcal{N}, \epsilon) = \left\{ y \in \mathcal{N} : d_{\mathcal{N}}(x, y) \leq \epsilon \right\}.$$

where $d_{\mathcal{N}}(x, y)$ is the distance of x and y on \mathcal{N} . For any positive integer number $k < m$, and any point $x \in \mathcal{M}$, let $\text{SubM}(x, \epsilon, k, \mathcal{M})$ be the set of all k -dimensional sub-manifolds of $\mathbf{B}(x, \mathcal{M}, \epsilon)$.

For a given k , the main idea of our principal sub-manifold is that at each point B of the sub-manifold \mathcal{N} , the sub-manifold should be able to explain the manifold variation as much as possible. To measure the degree of such variation for a potential sub-manifold, we introduce the angle α_B between the two hyperplanes, $H_k(B, \mathcal{M})$ and $H_k(B, \mathcal{N})$. Theoretically, if $\alpha_B = 0$ for every B , then $H_k(B, \mathcal{M}) = H_k(B, \mathcal{N})$. For general cases, one would hope α_B is as small as possible. This is in line with the fact that in the principal flow, on each point of the curve the tangent vector bends towards the tangent hyperplane at the same point. Therefore, an ideal definition of the sub-manifold will be

$$\arg \sup_{\mathcal{N} \in \text{SubM}(A, \epsilon, k, \mathcal{M})} \int_{B \in \mathcal{N}} \left(\cos(\alpha_B) \times \sum_{j=1}^k \lambda_j(B, \mathcal{M}) \right) d\mu_{\mathcal{N}}, \quad (2.9)$$

where $\mu_{\mathcal{N}}$ is the Lebesgue measure on \mathcal{N} .

As we can see, the principal sub-manifold in (2.9) is not attached to any specific parameterization of the sub-manifold \mathcal{N} . However, working with this definition requires integrating

on the surface without knowing its parameterization, which can be quite challenging. Recall that in (2.6), one can reparameterize the curve so that its velocity is a unit vector. This allows comparing curves to curves by their length. For sub-manifold in (2.9), where the integral would be taken over a multi-dimensional surface, having a unit speed parameterization of the surface is quite complicated. This means that comparing surfaces to surfaces is no longer applicable. Moreover, unlike the principal flow, that is invariant of reparameterization under the integration, the sub-manifold does not enjoy this property.

To avoid getting into too much technical details in parameterizing the sub-manifold, we change the Definition (2.9) slightly by 1) mapping \mathcal{N} onto the tangent space and 2) parameterizing the sub-manifold by polar coordinates. The idea is to apply the mapping to map \mathcal{N} into a ball of radius ϵ in its tangent space, and then we can use the polar coordinates of that ball in the tangent space. In line with the two steps, we gradually advance the definition of the principal sub-manifold and arrive at two definitions. The two definitions which are inter-connected with each other are summarized as Definition 2.3 and Definition 2.4. The connection between the two definitions will be further illustrated in Figure 2.

Denote $L(\mathcal{N}, \epsilon) = \log_p(\mathcal{N})$ to be the image of the sub-manifold \mathcal{N} at p under the logarithm map. The following definition naturally relax the ideal sub-manifold by replacing the integral with that being restricted on the image of the sub-manifold; that is, $d\mu_{\mathcal{N}}$ in (2.9) is replaced by $d\mu_k$. This modification allows us to have a more concrete sub-manifold in the sense that we do not need to deal with integration over \mathcal{N} .

Definition 2.3 *The k -dimensional principal sub-manifold is defined as follows*

$$\arg \sup_{\mathcal{N} \in \text{SubM}(A, \epsilon, k, \mathcal{M})} \int_{\log_A(B) \in \log_A(\mathcal{N})} \left(\cos(\alpha_B) \times \sum_{j=1}^k \lambda_j(B, \mathcal{M}) \right) d\mu_k,$$

where μ_k is the Lebesgue measure on the ball of the k -dimensional space of radius ϵ .

From Definition 2.3 (or see Figure 2 (b)), we see that when $k = 1$, the sub-manifold \mathcal{N} is a curve, and the tangent space $T_B \mathcal{N}$ at B reduces to the tangent vector v_B of the curve \mathcal{N} at point B . In this case, it is not difficult to see that $H_1(B, \mathcal{N})$ is the first eigenvector at B of the covariance matrix $\Sigma_{B, \mathcal{M}}$, and hence the measure of B on \mathcal{N} , $\mu_{\mathcal{N}}(B)$, becomes the length of the curve \mathcal{N} (or see Figure 2 (a)). This is equivalent to the definition of principal flow in Definition 2.6. Therefore, the principal sub-manifold is indeed an extension of the principal flow to the higher dimensional scenario, where $k \geq 2$.

In Theorem 1, we show that principal sub-manifolds (under Definition 2.3) are canonical, in the sense that they reduce to the usual principal components, in the context of Euclidean spaces. The proof of the theorem can be found in the Appendix.

THEOREM 1 *Assume that $\mathcal{M} = \mathbb{R}^d$ then*

$$\begin{aligned} \arg \sup_{\mathcal{N} \in \text{SubM}(A, \epsilon, k, \mathcal{M})} & \int_{\log_A(B) \in \log_A(\mathcal{N})} \left(\cos(\alpha_B) \times \sum_{j=1}^k \lambda_j(B, \mathcal{M}) \right) d\mu_k \\ &= \text{Hyperplane spanned by } \{e_1(A, \mathcal{M}), e_2(A, \mathcal{M}), \dots, e_k(A, \mathcal{M})\}. \end{aligned}$$

As seen, Definition 2.3 well relates to the principal flow. To actualize the Definition 2.3, the tangent space of \mathcal{N} should be further parameterized so that integration is applicable.

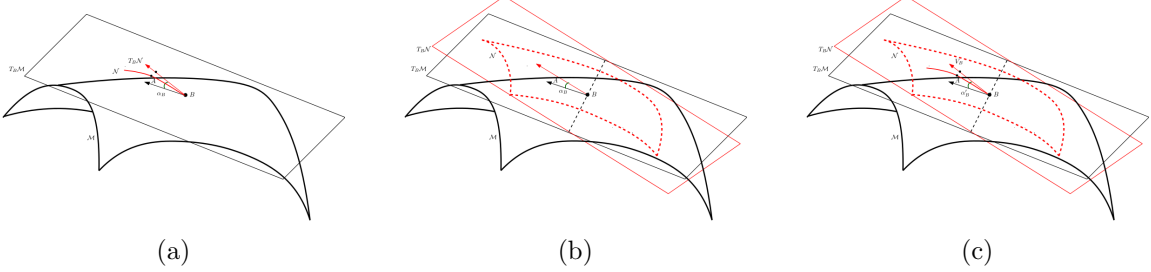


Figure 2: Principal sub-manifolds. (a) Principal flow; (b) Principal sub-manifold (Definition 2.3); (c) Principal sub-manifold (Definition 2.4)

To be precise, since $L(\mathcal{N}, \epsilon)$ belongs to a sphere with radius ϵ , for any point $B \in L(\mathcal{N}, \epsilon)$, there exists a unique point D such that $D = \exp_A(B)$ in \mathcal{N} . It makes sense that we parameterize $L(\mathcal{N}, \epsilon)$ using polar coordinates. For any point $B \in \mathcal{N}$, let v_B be the tangent vector field of a geodesic curve on the sub-manifold \mathcal{N} from A to B , denote α'_B to be the angle between v_B and hyperplane $H_k(B, \mathcal{M})$ (Figure 2 (c)). Here α'_B is chosen to replace α_B . Although α'_B does not necessarily equal α_B for every B , this modification not only measures how \mathcal{N} differs from \mathcal{M} at B , but also provides a convenient construction of a surface of maximal ‘‘cumulative variation.’’ Arguably, it appears to be more natural to work with this definition, as the integral can be approximated based on the polar coordinates.

Definition 2.4 *The k -dimensional principal sub-manifold is defined as follow*

$$\arg \sup_{\mathcal{N} \in \text{SubM}(A, \epsilon, k, \mathcal{M})} \int_{\log_A(B) \in \log_A(\mathcal{N})} \left(\cos(\alpha'_B) \times \sum_{j=1}^k \lambda_j(B, \mathcal{M}) \right) d\mu_k,$$

where μ_k is the Lebesgue measure on the ball of the k -dimensional space of radius ϵ .

Remark Definition 2.4 is almost identical to Definition 2.3. A similar theorem for Definition 2.4 could be easily stated and proved; hence we omit them.

We conclude this session with a remark on the interpretation of Theorem 1. In comparison with the principal flow, recall the similar result in principal flow (Proposition 5.1, [19]) where the first order of the principal flow on a flat space has been shown to coincide with the first principal direction with a condition that the locality parameter of the tangent covariance matrix is chosen to be infinity. Higher order principal flows will no longer necessarily reduce to the principal components when local tangent covariance is employed in flat space. The result of Theorem 1 for principal sub-manifold does not require this condition.

3 Determination of Principal Sub-manifold

3.1 An algorithm for two-dimensional principal sub-manifold

At this point, we remark here that there is no fundamental difference of working with a two-dimensional sub-manifold or a higher one from a theoretical view. We will discuss how to determine the following two-dimensional principal sub-manifold (e.g., $k = 2$ of Definition 2.4) as a special case and present an algorithm for the rest of paper. The extension of the algorithm derived here to any multi-dimensional sub-manifold is obvious.

Definition 3.1 *The two-dimensional principal sub-manifold is defined as follow*

$$\arg \sup_{\mathcal{N} \in \text{SubM}(A, \epsilon, 2, \mathcal{M})} \int_{\log_A(B) \in \log_A(\mathcal{N})} \cos(\alpha'_B) \times \left(\lambda_1(B, \mathcal{M}) + \lambda_2(B, \mathcal{M}) \right) d\mu_k,$$

where μ_k is the Lebesgue measure on the ball of the k -dimensional space of radius ϵ .

The principal flow is the solution of an optimization problem defined in Definition (2.6) or (2.7). To find such a solution, it requires extensive searching for a critical point of a Euler-Lagrange problem that involves integrating the vector field along the curve. And because it is a one dimensional curve, numerical methods are coincidentally helpful as shown in [19], in that it reduces to a problem of determining the solution of a system of ordinary differential equations (ODEs). However, when it comes to a sub-manifold, things turn out to be quite different. In particular, we have not found a numerically efficient solution to the corresponding optimization problem for the sub-manifold defined in Definition 3.1. The main reason is that, one needs a much more sophisticated Lagrange formulation to optimize over a chosen sub-manifold with a very different initial condition; whereas in the case of principal flow one only needs a starting point and an initial speed.

We will avoid optimizing the integral in Definition 3.1 directly. Instead, to find a smooth principal sub-manifold \mathcal{N} , we will take a very different strategy: to find an approximated solution. The essence of our approach is to represent \mathcal{N} by a collection of ordered nets of sub-manifolds, with each one comprising a sequence of *small* sub-manifolds. The sub-manifolds within each sequence are to represent certain amount of data variation along a certain direction of \mathcal{N} . The sub-manifolds are expected to grow and expand along all directions. From this perspective, our approach attains an approximated solution and it involves no optimization. To calculate such an approximated solution, we start from a point $A \in \mathcal{M}$, and name it as the 1st Level of all *nets* of the sub-manifolds. The choice of A can be the same as that in principal flow. Note that the principal flow moves restrictively along the first principal direction of data variation. In this sense, those directions that the sub-manifolds would expand provide an extra dimension to build up the target sub-manifold. Many of such nets of sub-manifolds at different levels representing an approximation to the sub-manifold \mathcal{N} at A —in every possible direction of variation—remain to be found. To obtain each net of the sub-manifolds, one needs to parameterize all the directions on the tangent space at A . Let $H_2(A, \mathcal{M})$ be the tangent plane spanned by $e_1(A)$ and $e_2(A)$ of the covariance matrix $\Sigma_{A, \mathcal{M}}$, or more favorably the local covariance matrix $\Sigma_{h, A, \mathcal{M}}$. We will neglect the subscript \mathcal{M} and only use $\Sigma_{h, A}$ for a better presentation. To make a local move in different directions, we propose to form a circle of radius ϵ on the tangent plane $H_2(A, \mathcal{M})$ centered at A . This is equivalent to choosing the points Z_θ on the circle

$$\epsilon \times \left[\cos(\theta) e_1(A) + \sin(\theta) e_2(A) \right], \quad 0 \leq \theta \leq 2\pi,$$

and then mapping them back to the manifold via $A_\theta = \exp_A(Z_\theta)$. Here, the subscript θ denotes the direction θ on the tangent plane for each move. We grow the net of the sub-manifolds along each direction, and project them similarly along the way. In the end, we call all the nets of the sub-manifolds for all directions a *principal sub-manifold* \mathcal{N} .

Remark: there is no difference in either forming a circle or an ellipse for small ϵ . In case of an ellipse, the axes of ellipse would be proportional to the first and second eigenvalue of $\Sigma_{h, A, i}$.

To discretize θ , let $\theta = 2l\pi/180, 1 \leq l \leq 180$. For each direction l , we are going to build a sequence

$$(A_{l,0}, A_{l,1}, A_{l,2}, A_{l,3}, \dots)$$

with the starting points $A_{l,0} = A$ and $A_{l,1} = A_l$.

Here, we elaborate the core of the algorithm (See Algorithm 1 for a detailed description): suppose that given direction l , we are at the i th Level, $A_{l,i}$, there are three steps needed to go through to find the $(i+1)$ th Level of principal sub-manifold $A_{l,i+1}$

- (1) *Transports on the tangent plane*: expand the points $A_{l,i}$ in each direction l by a step of ϵ
- (2) *Projection*: update the points $A_{l,i}$ along the highest curvature locally and arrive at points $A_{l,i+1}$
- (3) *Updating*: at each direction l , project the data points x_j 's ($1 \leq j \leq n$) onto the new extended point $A_{l,i+1}$, and re-calculate the tangent plane at $A_{l,i+1}$

In step (1), based on $A_{l,i}$, we are going to pick points on the circle centering at $A_{l,i}$

$$u_{l,i} = \langle v_{l,i}, e_1(A_{l,i}) \rangle e_1(A_{l,i}) + \langle v_{l,i}, e_2(A_{l,i}) \rangle e_2(A_{l,i})$$

where $v_{l,i} = \log_{A_{l,i}}(A_{l,i-1})$. Here $e_1(A_{l,i})$ and $e_2(A_{l,i})$ are the first and second eigenvector of $\Sigma_{h,A_{l,i}}$.

In step (2), project the new local points along the highest curvature

$$r_{l,i} = \epsilon \times \frac{u_{l,i}}{\|u_{l,i}\|},$$

and then map them back to the manifold \mathcal{M}

$$A_{l,i+1} = \exp_{A_{l,i}}(-r_{l,i}).$$

Therefore, $A_{l,i+1}$ is an image of $u_{l,i}$ under the exponential map.

In step (3), at every current Level i , the move for the next Level $i+1$ is guided by the local structure of the data points at the current level. In this sense, the covariance matrix $\Sigma_{h,A_{l,i}}$ needs to be updated by $\Sigma_{h,A_{l,i+1}}$.

It is crucial to make sure that the principal sub-manifold always moves forward, and never moves backward to the points it has already explored. In the meanwhile, a stop condition is also necessary. Denote the l th net of sub-manifolds as

$$\mathcal{A}_l = (A_{l,0}, A_{l,1}, A_{l,2}, \dots, A_{l,N(l)})^T \quad (3.10)$$

where $N(l)$ is the number of the levels before it stops. The l th net of the sub-manifolds contains the points that have been explored along the direction l . This can be seen as an effect of cumulative variation. In accordance with the stopping rule used in [19], we can terminate the process when the *length* of the l th net, i.e.,

$$\ell_{\mathcal{A}_l} = \sum_{i=1}^{N(l)-1} d(A_{l,i}, A_{l,i+1}),$$

exceeds 1. The length of l th net does not necessarily have to be equal. There may exist other stopping rules that one can use. Among them, we should also consider that for all j ,

$$\|\log_{A_{l,i+1}}(x_j)\| > \delta \text{ or } \langle \log_{A_{l,i+1}}(A_{l,i}), \log_{A_{l,i+1}}(x_j) \rangle \geq 0,$$

which implies that either there are not enough data points in the neighborhood or $A_{l,i+1}$ is already outside the convex hull of the x_j 's under the logarithm map.

Remark both ϵ and δ are pre-defined parameters. We suggest to choose ϵ favorably with small values, as in this case, small values of ϵ ensure the stability of the local move on the tangent plane, while the choice of δ depends more on the data dispersion and configuration, which might vary from case to case.

Algorithm 1: two-dimensional principal sub-manifold

1. At a point A (mean or other point), use the logarithm map: $\log_A(x_i) = y_i$.
2. Find the covariance matrix from y_1, \dots, y_n

$$\Sigma_{h,A} = \frac{1}{\sum_i (\|y_i - A\| \leq h)} (y_i - A)^T (y_i - A).$$

3. Let $e_1(A)$ and $e_2(A)$ be the first and second eigenvector of $\Sigma_{h,A}$. Define

$$Z_l = \epsilon \times \left[\cos(2l\pi/180) e_1(A) + \sin(2l\pi/180) e_2(A) \right],$$

with $l = 1, \dots, 180$.

4. Use exponential map to map Z_l on the manifold so we get a set of new points $\exp_A(Z_l) = A_l$.
5. Assume that we stay at point $A_{l,i}$, we are going to find $A_{l,i+1}$ ($A_{l,0} = A$ and $A_{l,1} = A_l$) via steps (a)-(g)

(a) find $\Sigma_{h,A_{l,i}}$.

(b) find $e_1(A_{l,i})$ and $e_2(A_{l,i})$.

(c) find $v_{l,i} = \log_{A_{l,i}}(A_{l,i-1})$.

(d) find

$$u_{l,i} = \langle v_{l,i}, e_1(A_{l,i}) \rangle e_1(A_{l,i}) + \langle v_{l,i}, e_2(A_{l,i}) \rangle e_2(A_{l,i})$$

where $\langle a, b \rangle = \sum_{i=1}^n a_i b_i$ with $a = (a_1, \dots, a_n)$ and $b = (b_1, \dots, b_n)$.

(e) calculate

$$r_{l,i} = \epsilon \times \frac{u_{l,i}}{\|u_{l,i}\|}.$$

(f) update

$$A_{l,i+1} = \exp_{A_{l,i}}(-r_{l,i}).$$

(g) stop at $A_{l,i+1}$ when

$$\langle \log_{A_{l,i+1}}(A_{l,i}), \log_{A_{l,i+1}}(x_j) \rangle \geq 0.$$

for all $j = 1, \dots, n$.

6. For every $l = 1, \dots, 180$, connect $A_{l,i}$ with $A_{l,i+1}$ by i we get a net of principal sub-manifold.

7. **Output:** all A_l 's as in (3.10), where $1 \leq l \leq 180$.

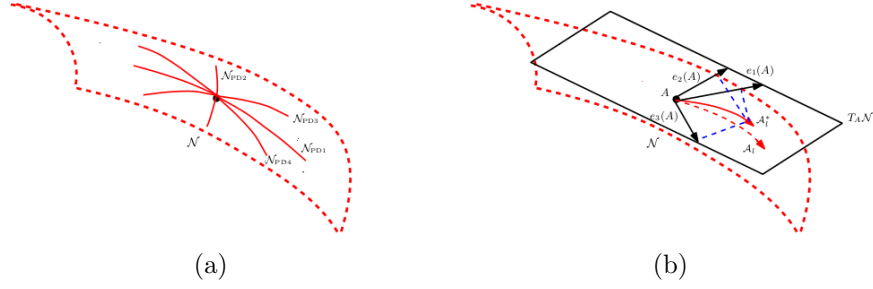


Figure 3: Visualization of a principal sub-manifold. (a) Visualize the sub-manifold by the five principal directions. (b) Visualize the sub-manifold by projecting to the three largest eigenvectors of covariance matrix at A .

3.2 Visualization of the principal sub-manifold

The principal sub-manifold in general cannot be fully visualized when its dimension exceeds one. Consider a simple case where the data lies in $S^3 \subset \mathbb{R}^4$; the principal sub-manifold is then a subset of S^3 ; that is, it is equivalent to visualizing a two-dimensional manifold in a four-dimensional space. However, a meaningful representation of the sub-manifold is still quite relevant for understanding the manifold variation, at least partially. We propose two ways of visualizing the principal sub-manifold. The first one is to represent the sub-manifold in the principal directions. The second one is to visualize the sub-manifold in the projected manifold space.

- parameterize the sub-manifold in polar coordinates and represent it by the shapes of the principal directions
- project the sub-manifold by multiplying a rotation matrix in which the basis is formed by eigenvectors from the covariance matrix at the starting point

Visualization in principal direction: We aim to choose the most varying parts of sub-manifold and visualize the sub-manifold by using these very parts. To see this, let's first denote the entire sub-manifold, obtained by Algorithm 1, as follows

$$\mathcal{N} = [\mathcal{A}_1, \mathcal{A}_2, \dots, \mathcal{A}_{180}]^T$$

Although we call \mathcal{N} as a “matrix”, the actual length of each row (i.e., $\mathcal{A}_l, 1 \leq l \leq 180$) may vary. To visualize the sub-manifold, we select a candidates set \mathcal{L} and transform the corresponding rows of \mathcal{N} to the corresponding shape coordinates. The idea is to present the most varying parts of sub-manifold by

$$x_{l,j} = f^{-1}(A_{l,j}), \quad \forall l \in \mathcal{L}, 1 \leq j \leq N(l),$$

where f is the embedding defined in Kendall shape space (Section 2.4). Note that the resultant $x_{l,1}, \dots, x_{l,N(l)}$ is a collection of $N(l)$ k -ads.

Among all directions, we call the following two directions as the *principal directions* of the sub-manifold. The first principal direction, denoted as $\mathcal{N}_{\text{PD}1}$, is the curve corresponding to $\theta = \pi$ and $\theta = 2\pi$ with its image positioned on the tangent plane. Under the polar coordinate parameterization, this is equivalent to l equals 90 and 180 such that

$$\mathcal{N}_{\text{PD}1} = \mathcal{A}_{90} \cup \mathcal{A}_{180}.$$

The second principal direction, denoted as $\mathcal{N}_{\text{PD}2}$, corresponds to the curve with $\theta = \pi/2$ and $\theta = 3\pi/2$ with its image positioned on the tangent plane. Under the same parameterization, this is equivalent to l equals 45 and 135 such that

$$\mathcal{N}_{\text{PD}2} = \mathcal{A}_{45} \cup \mathcal{A}_{135}.$$

Since $\mathcal{N}_{\text{PD}1}$ and $\mathcal{N}_{\text{PD}2}$ are indeed curves on \mathcal{N} , they should not be interpreted as the usual principal components in Euclidean space. The “principal” in the notation of $\mathcal{N}_{\text{PD}1}$ and $\mathcal{N}_{\text{PD}2}$ is canonical in the sense that the images of the two curves, at least locally, correspond to the principal components on the tangent space.

In principal, the set \mathcal{L} should include at least the two principal directions. In addition, it is suggested to also include the curves, $\mathcal{N}_{\text{PD}1}$, corresponding to $\theta = \pi/4$ and $\theta = 5\pi/4$ as well as the ones, $\mathcal{N}_{\text{PD}4}$, corresponding to $\theta = 3\pi/4$ and $\theta = 7\pi/4$. Adding two extra directions gives extra details about the sub-manifold. We remark that although we have used $\mathcal{N}_{\text{PD}3}$ and $\mathcal{N}_{\text{PD}4}$ implicitly as the third and fourth principal directions, they are by no means the third and fourth principal components on the tangent space. Figure 3(a) gives an example of such a configuration of shapes. The entire image contains 9 by 9 small shapes. The central figure is the mean shape. Row 5 represents the shapes of $\mathcal{N}_{\text{PD}1}$. Column 5 is the shapes of $\mathcal{N}_{\text{PD}2}$. The main diagonal contains the shapes of $\mathcal{N}_{\text{PD}3}$. The other diagonal contains the shapes $\mathcal{N}_{\text{PD}4}$.

Visualization in projected space: Alternatively, one may wish to represent the sub-manifold using a projected sub-manifold rather than itself. The projected sub-manifold serves as a much simplified version of the original one and it is more interpretable, provided the majority of variation of the principal sub-manifold can be explained by a reduced one; that is, the l th net of the sub-manifold, $A_{l,i}$, would be reasonably explained under a small number of largest eigenvectors at Σ_A . Compared to the previous representation, this visualization remains the resolution of the sub-manifold. Suppose the principal sub-manifold \mathcal{N} is obtained by Algorithm 1, we center the \mathcal{N} row-wise by the starting point A and obtain the centered sub-manifold as

$$\mathcal{N}^* = (\mathcal{N}_{l,j}^*)_{1 \leq l \leq 180, 1 \leq j \leq N(l)}$$

where $\mathcal{N}_{l,j}^* = A_{l,j} - A$ where $1 \leq l \leq 180, 1 \leq j \leq N(l)$. Note that for $j = 1$, $\mathcal{N}_{l,1}^* = \mathbf{0}$. Then, \mathcal{N}^* is projected to a new coordinate system consisting of the first few eigenvectors of Σ_A . The projection is defined as follows

$$\Psi = (\psi_{l,j})_{1 \leq l \leq 180, 1 \leq j \leq N(l)}, \quad \psi_{l,j} = E_3$$

where $E_3 = [e_1(A), e_2(A), e_3(A)]^T$ of Σ_A . The process is carried out by multiplying element-wise; \mathcal{N}^* by the projection Ψ , so that

$$\mathcal{N}^{\text{pro}} = \Psi \odot \mathcal{N}^*$$

where \odot is the element-wise product such that $\mathcal{N}_{l,j}^{\text{pro}} = \psi_{l,j} \mathcal{N}_{l,j}^*$. Figure 3(b) illustrates the main idea: the red dashed arrow starting from A denotes the l th net (or a vector of $(A_{l,1}, \dots, A_{l,N(l)})$) of the principal sub-manifold \mathcal{N} ; the red solid arrow denotes the projected l th net of the principal sub-manifold. The point A on the sub-manifold \mathcal{N} (3) is regarded as the origin under the new coordinate system, correspondingly. Moreover, the data points x_i ’s are projected in the same way by

$$x_i^* = E_3(x_i - A), \quad 1 \leq i \leq n.$$

In principal, the projected points x_i^* 's are expected to lie closely to the sub-manifold \mathcal{N}^{pro} , provided that the projection matrix has accounted most of the variability.

3.3 A demonstration of the algorithm

To illustrate the principal sub-manifold, we generate a set of data points from a curved surface in $S^3 \subset \mathbb{R}^4$. The data is originally constructed by sampling the triplets $(x_{i,1}, x_{i,2}, x_{i,3}) \subset \mathbb{R}^3$ from the distribution

$$\begin{pmatrix} x_{i,1} \\ x_{i,2} \\ x_{i,3} \end{pmatrix} = \begin{pmatrix} (i - n/2)/n \\ \sin(2x_{i,1})/6 + 32U \\ 1 + 1/100V \end{pmatrix}, \quad 1 \leq i \leq n$$

where U and V are independent normal variable $N(0, 1/10)$ and $N(0, 1/100)$. To lift each point to \mathbb{R}^4 , we add the fourth coordinate so that every point lies on a sphere satisfying

$$x_{i,1}^2 + x_{i,2}^2 + x_{i,3}^2 + x_{i,4}^2 = C,$$

where a shifting parameter C (e.g., 0.45) is chosen such that

$$\sqrt{C - x_{i,1}^2 - x_{i,2}^2 - x_{i,3}^2} \geq 0.$$

We still need to normalize the data to guarantee that the data are in S^3 .

The curved surface gives some knowledge about the inherited geometry of the projected sub-manifold. This can be understood by noting that the surface carries an S -pattern that mainly comes from a rough sinusoid of the triplets. Figure 4 shows the data, the estimated principal sub-manifold, and the super-imposed principal directions. The starting point (in black) is the center of the data points (in red). The two green curves are the first and second principal direction lying on the surface corresponding to the estimated principal sub-manifold (in grey). All of them are projected to the first three eigenvectors of the covariance matrix at the starting point. The surface enables itself to bend wherever the curvature of the manifold changes rapidly. The first principal direction is towards a direction of maximum variance of the data points, while the surface grows in more directions that automatically account for more variance of the data points.

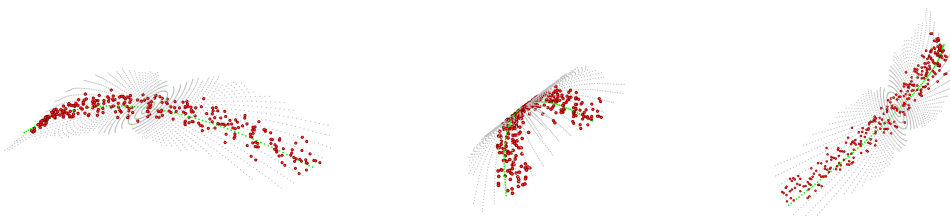


Figure 4: Visualization of the projected two-dimensional sub-manifold for data on S^3 , from three different view points. The data points are labeled in red, with the first and second principal direction (in green) going through the starting point. The sub-manifold (in gray) are constructed by Algorithm 1. For visualization purpose, the sub-manifold, the first and second principal direction and the data points have been projected to the first three eigenvectors of the covariance matrix at the starting point.

4 Examples

This section contains a set of simulated data sets and two real data sets that illustrate the use of the principal sub-manifold.

4.1 Simulated Data

To further investigate the behavior of the principal sub-manifold as dependent on the configuration of the data points and the choice of scale parameter, we considered three sets of examples on S^3 . We chose this surface as a “test manifold” since it represents one of the most natural spaces from which the projected sub-manifold can be well understood, and since it provides a manifold for which we can compare the principal sub-manifolds with the principal geodesic. We observe here that the full manifold variation of the sub-manifold from the data can be very complicated; hence, we do not look at them on a quantitative basis, but rather investigate them qualitatively.

The first set of examples involves five data clouds in S^3 with each presenting a different curvature. As the curvature is non-constant, the Fréchet mean is no longer a good starting point for the principal sub-manifold. Instead, we choose the center of symmetry for each data as a starting point. The first and second data cloud are constructed in a way that the first three coordinates of each point are concentrated around a one dimensional curve; the configuration of the third and fourth are such that the points are on a two-dimensional surface/plane; the fifth one is much more diffuse: the points lie on a sea-wave-like surface.

For each one of them, a two-dimensional principal sub-manifold was fitted using three different h and the results are presented. The results indicate that the corresponding sub-manifolds perform well in capturing the local and global variation. We note that the sub-manifold fits well for data Cloud 1 no matter what scale of h is used (Figure 6(a)-(c)); the sub-manifold seems to capture a finer structure with a reduced value for h for data Cloud 2 (Figure 6(d)-(f)): this can be also seen as the first principal direction evolves with the scale of h . When the surface becomes two-dimensional for data Clouds 3 and 4, the principal sub-manifolds also excel: the fitted sub-manifold remains unchanged for different h as the surface is flat (Figure 6(g)-(i)), while it picks up the appropriate structure with a reduced h for bended surface (Figure 6(j)-(l)); For the cloud 5 (Figure 6(m)-(o)), it is more obvious that using a sub-manifold is more appealing than using only a curve or its equivalent; the sub-manifold fits the data points surprisingly well even with a surface of high curvature.

To contrast the principal sub-manifold with the standard principal geodesic, we include the results of principal geodesics for the case of Figure 5(j) and Figure 5(m). Specifically, the best h has been chosen for either method to perform appropriately. It is expected that the principal geodesic, essentially a principal great circle, is not capable of capturing the curvature; that is, the two principal geodesics (in black) for both cases (Figure 7(a)) and (Figure 7(b)) tend to deviate from the principal directions (in green) shortly after the starting point, thus not lying on the surface. In contrast, the principal sub-manifold handles the curvature well in both cases.

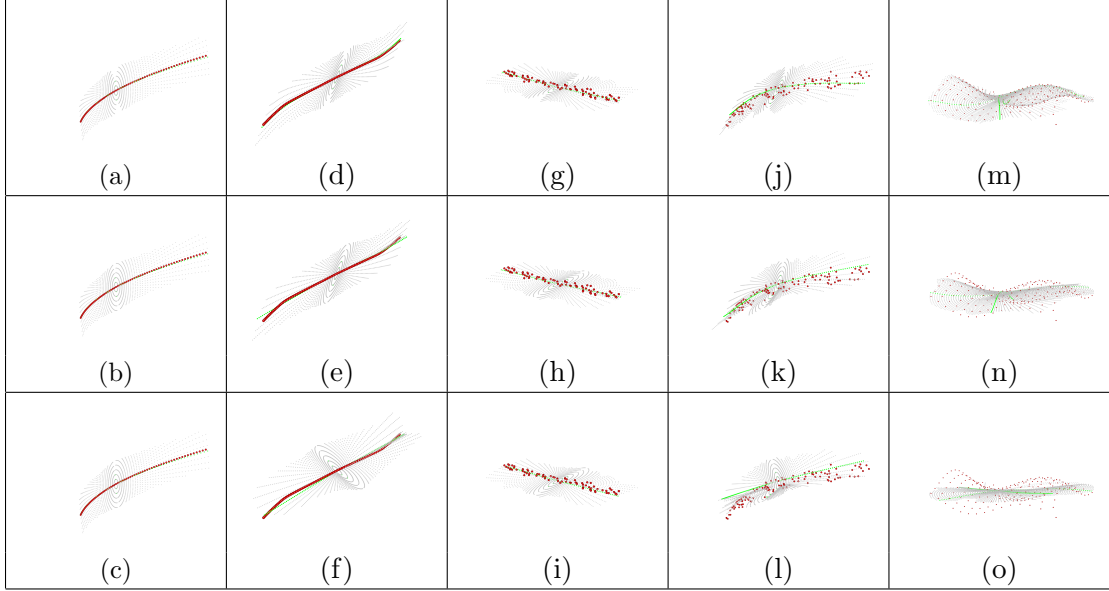


Figure 5: Principal sub-manifolds (with superimposed principal directions) for five data clouds in S^3 , with different scale parameters. (a)-(c) Principal sub-manifolds (in gray) and principal directions (in green) for data Cloud 1 (in red) for different values of h (small, middle, large). (d)-(f), (g)-(i), (j)-(l) and (m)-(o) provide the same information for data Clouds 2, 3, 4 and 5.

To probe how a sub-manifold performs with a noisy surface, we created four sets of data by blurring the sea-wave-like surface aforementioned with increasing levels of noise. Although the data reside in S^3 , most of the variation originates around a surface but not exactly on the surface. By knowing how the data points lie around the surface, we can get a sense of such variability. As we should no longer look at the local scale when the points tend to have large variability, we found a two-dimensional sub-manifold by choosing an appropriate scale parameter h , potentially a larger one, for each data set. In Figure 6(a), when there is no noise, it is expected that the sub-manifold would capture total variation of the data in the projected space. When the noise increases (Figure 6(b) (c), and (d)), where all points are more diffused away from the underlying projected surface, the fitted sub-manifold is, although not a perfect sub-manifold, still well explaining for total data variability.

The last sets of examples are from a “lifted” ellipsoid in S^3 . Intuitively, the four data sets we generated represent different but inter-connected types of situation: (1) the triplets are well spread out inside the ellipsoid; (2)-(3) the triplets are mostly being concentrated in the middle of a more flatter ellipsoid; (4) the triplets are chosen nearly on the diameter of the ellipsoid (potentially around an ellipse). For case (1) (Figure 8(a)), where most points are inside the ellipsoid, neither one-dimensional nor two-dimensional sub-manifold would be a perfect sub-manifold. As the diffusion decreases, such as in case (2) (Figure 8(b)) and (3) (Figure 8(c)), the sub-manifold of dimension two appears to be more and more appropriate. In case (4) (Figure 8(d)), the sub-manifold provides the best fit such that all the projected data points lie on the sub-manifold. As one has already observed, the contribution of a two-dimensional sub-manifold in this example is only marginal. Arguably though, one can go further, for instance, having a higher dimensional sub-manifold in case (1) or case (2). Such extension of the algorithm would be very natural, but the details of implementing the algorithm are quite subtle and we choose not to proceed further.

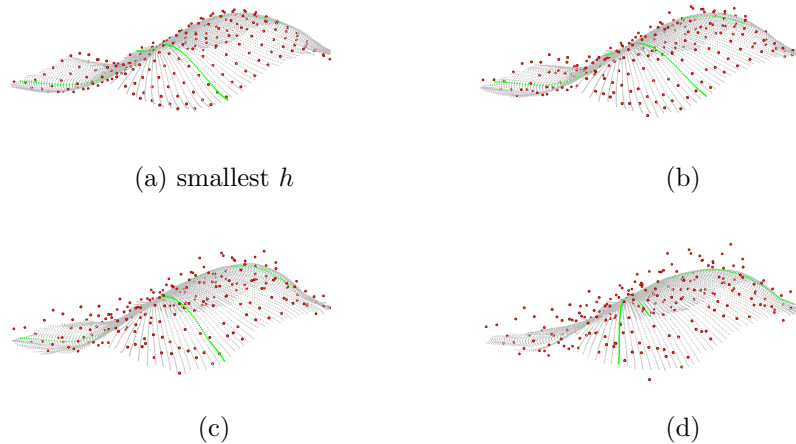


Figure 6: Principal sub-manifolds (with superimposed principal directions) for four sea wave sets of data with noise on S^3 . (a) Principal sub-manifolds with no noise added. (b), (c) and (d) provide the same information for three different noise levels.

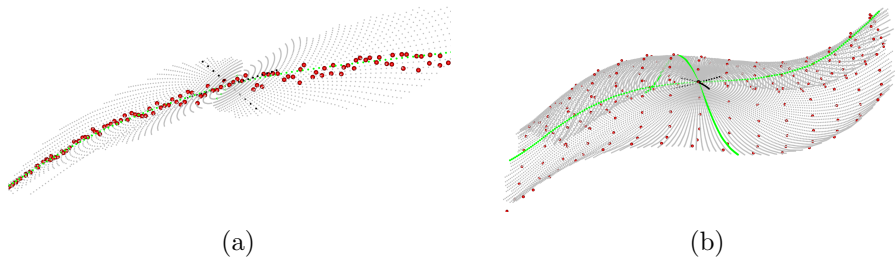


Figure 7: Comparison of principal sub-manifolds and principal geodesics. The principal geodesics (in black) are superimposed to the principal directions (in green) in the projected space. Only segments of the principal geodesics are highlighted for visualization purpose.

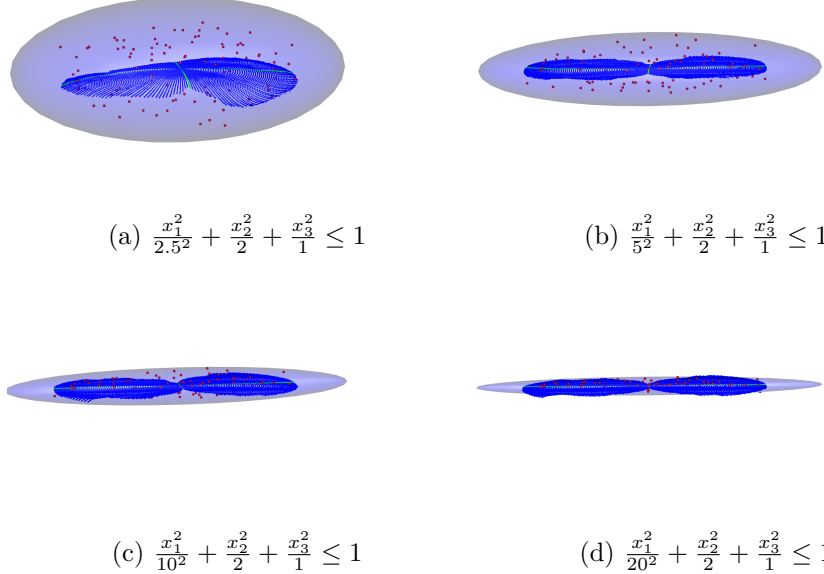


Figure 8: Principal sub-manifolds (with superimposed principal directions) for four ellipsoid sets of data on S^3 . (a) Principal sub-manifolds (in blue) and principal directions (in green) for data set (in red) of case (1). (b), (c) and (d) provide the same information for case (2), (3) and (4).

4.2 Principal variation of handwritten digits

To illustrate the use of the principal sub-manifold in a concrete example, we first consider a handwritten digit “3” data. The data, available at <https://www.maths.nottingham.ac.uk/personal/ild/bookdata/digit3.dat>, consists of 13 landmarks of a “3” in two dimensions, collected from 30 individuals. To visualize how the shape of the digit “3” varies, we find a principal sub-manifold for the data and recover the shape variation of the “3” in four principal directions, started at two different shapes of the “3”. In the first case (see Figure 10), the sub-manifold starts from the Fréchet mean of the data. In each principal direction, the flow of images describes the shapes of the ‘3’ moving from one extreme to the other extreme. The horizontal set of the images represents the various shapes of “3” recovered from the first principal direction. From there, we can see that the most varying part is the middle part of the “3.” The parts varying in the second principal direction are mainly the upper and lower parts of the “3.” Those parts of the “3” have exhibited a significant shape change along the two principal directions. Both, main diagonal and the other diagonal show certain degrees of the shape change mostly in the middle part of the “3” but in an opposite direction. By observing the fact that there are two seemingly outlying individuals of “3”s deviating from the rest in the data—the mean having moved away from the actual center of the data—a more sensible center of symmetry should be also considered. As the second case, Figure 11 serves to illustrate the slight effect of having a different choice of the starting point on the sub-manifold. However, no significant change in the representation of the sub-manifold is found.

4.3 Principal variation of leaf growth

We also considered a landmark data set consisting of leaf growth, collected from three Clones and a reference tree of young black Canadian poplars at an experimental site at the University of Göttingen. The landmark configurations of the leaves were collected from three Clones ('C1', 'C2', 'C3') and a reference tree ('r') collected at two different levels: breast height (Level 1) and the crown (Level 2). They consist of the shapes of 27 leaves (nine from Level 1 and eighteen from Level 2) from Clone 1; of 22 leaves (six from Level 1 and sixteen from Level 2) from Clone 2; and of 24 leaves (eighteen from Level 1 and seventeen from Level 2) from Clone 3 as well as of the shapes of 21 leaves (thirteen from Level 1 and eighteen from Level 2) from the reference tree, all of which have been recorded non-destructively over several days during a major portion of their growing period of approximately one month. There are four landmarks corresponding to quadrangular configuration at petiole, tip, and largest extensions orthogonal to the connecting line. Though Figure 9 represents the four landmarks extracted from the contour image of each leaf on a flat plane, the four landmarks contain, in particular, the information of length, width, vertical and horizontal asymmetry.

Although it is known that the leaf growth of the genetically identical trees along a period of time reveals a non-Euclidean pattern [12], the study only focused on the mean geodesic difference (therefore essentially a one-dimensional variation), which is used for the discriminant analysis across the trees. However, the shape change along different directions—especially the principal directions in shape space—has not been fully explored. We will investigate the shape variation using principal sub-manifold among three clones and the reference tree. As can be expected (see in Section 2.2), each landmark configuration, represented by a polygon in Figure 9, corresponds to a point in the *shape space* Σ_2^4 . We focus on the non-geodesic shape variation primarily in vertical and horizontal direction of the leaf growth, the analysis of which requires a multi-dimensional scale treatment.

As all the leaves are very young, we first combine the leaves from the breast height and crown for each tree. For each three, a principal sub-manifold is found, where two principal directions are extracted from the fitted sub-manifold. The two principal directions are then transformed to preshape space and all the landmarks recovered are superimposed. Results for all the three Clones and the reference tree are displayed in Figure 12. The leaves of the reference tree exhibit two main kinds of variation: the first one tends to follow the horizontal direction with some effects along the vertical direction at tip. This can be well seen by the first principal direction in Figure 12(a); the second one concentrates on petiole, which is displayed by the second principal direction in Figure 12(b). The three Clones reveal different patterns of variation from the reference tree; between, them each one differs from the other. Clone 1 shows more variation at the petiole and the left extension seen in the first principal direction, while the second principal direction shows more variation at the right extension; the two principal directions of the Clone 2 behave more similarly as that of the reference tree, with some other variation appearing in the second principal direction of the Clone 2 at the right extension and the tip; unlike Clone 1 and 2, variation in both vertical and horizontal directions appear evenly in either the first principal direction and the second principal direction for Clone 3. The same analysis for the leaves at breast height and crown alone has also been performed separately with a similar outcome, as shown in Figure 13, the result suggesting no different conclusion.

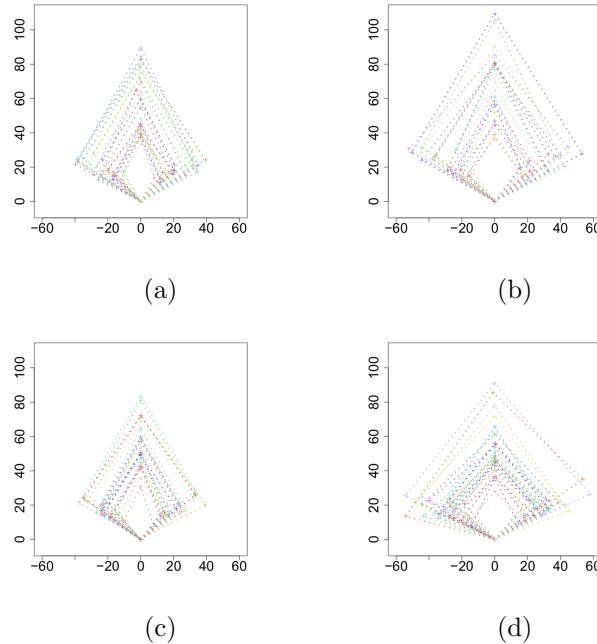


Figure 9: Leaf growth over a growing period of Clone 1 (a), Clone 2 (b), Clone 3 (c), and a reference tree (d). (a) Four landmarks on the leaf of clone 1 have been connected and represented by a polygon at each growing period (27 polygons totally); (b)-(d) provide the same information for Clone 2 (22 polygons), Clone 3 (24 polygons) and the reference tree (31 polygons).

5 Discussion

Due to the nature of the ways in which data is collected or recorded, the induced spaces are very often nonlinear manifolds. The statistical analysis of data on Riemannian manifold is a very challenging topic and it plays an increasingly important role in real-world problems. Conventional approaches, such as canonical PCA in Euclidean space, are essentially helpful in neither learning the shape of the underlying manifold nor deciding its dimensionality. The main reason for this lies in the fact that those approaches simply do not use the intrinsic Riemannian manifold structures.

With the aim of proposing a method that allows for finding a nonlinear manifold from the data, we introduced the notation of principal sub-manifold. We showed the importance of estimating a multi-dimensional sub-manifold, and its difference from finding only a one dimensional curve. The principal sub-manifold was seen to be interpretable as a measure of nongeodesic variation of the data. Based on a polar coordinate representation, the principal sub-manifold was constructed so that it coordinated with the local curvature. We illustrated that the principal sub-manifold is an extension of the principal flow, in the sense that it depicts a multi-dimensional manifold. When the manifold is linear, the principal sub-manifold reduces to the canonical principal components. In this sense, it can also be thought of as a manifold extension of the principal surface.

We claim here that by definition, the implemented principal directions might or might not coincide with the principal flows that are defined in [19], although in practice, they appear to be close to or the same as the principal flows. Under the polar coordinate

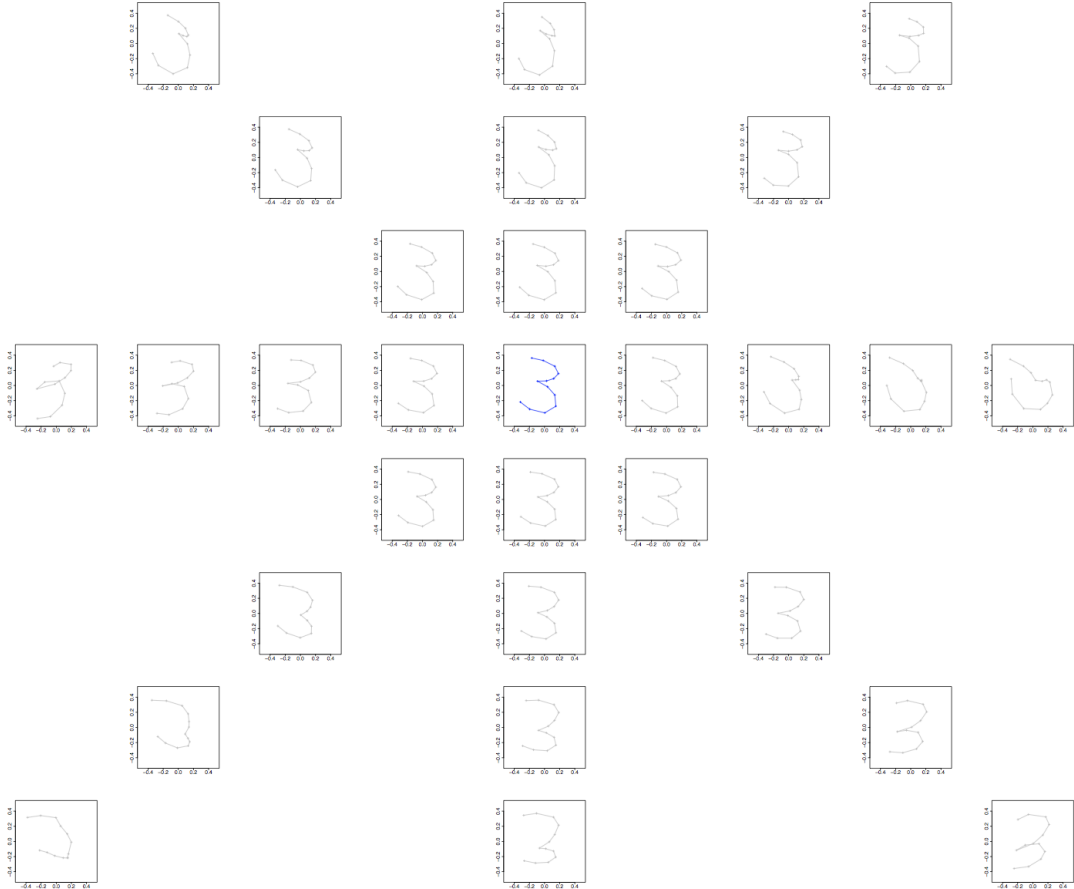


Figure 10: Principal sub-manifolds of the handwritten digits data, started from the mean. Among all the figures: the central figure (in blue) is the Fréchet mean; the horizontal row contains images recovered from the first principal direction of the sub-manifold; the vertical column is the second principal direction; the main diagonal is the third principal direction; the other diagonal is the fourth principal direction.

representation, we observe that the principal directions (these are plotted in green in Figure 4) on the principal sub-manifold have presented the main modes of variation.

Regarding the issue of choosing the locality parameter h , or equivalently, at which scale of the local covariance should one consider? Admittedly, different sub-manifolds would have been fitted by choosing different parameters. Still, we suggest not making a strict statement on optimizing the h ; rather, one should overview a sequence of h . We recommend the readers engage in a discussion of such choices associated with possible forms of criterion in [19] and the scale space perspective [1]. Simultaneously, we were able to define the principal sub-manifold to any dimension $k \leq d$, and this may also be seen as the development of a heuristic understanding of backward stepwise principle of PCA on manifolds: in the backward PCA, the best approximating affine subspaces are constructed from the highest dimension to the lowest one, see [14] for a spherical case of subspace, while in the case of principal sub-manifold, each net of the principal sub-manifolds (i.e., the principal directions) corresponds to the lower dimension sub-manifolds, compared to the entire sub-manifold.

Last but not least, the formulation of the principal sub-manifold opens the way to the

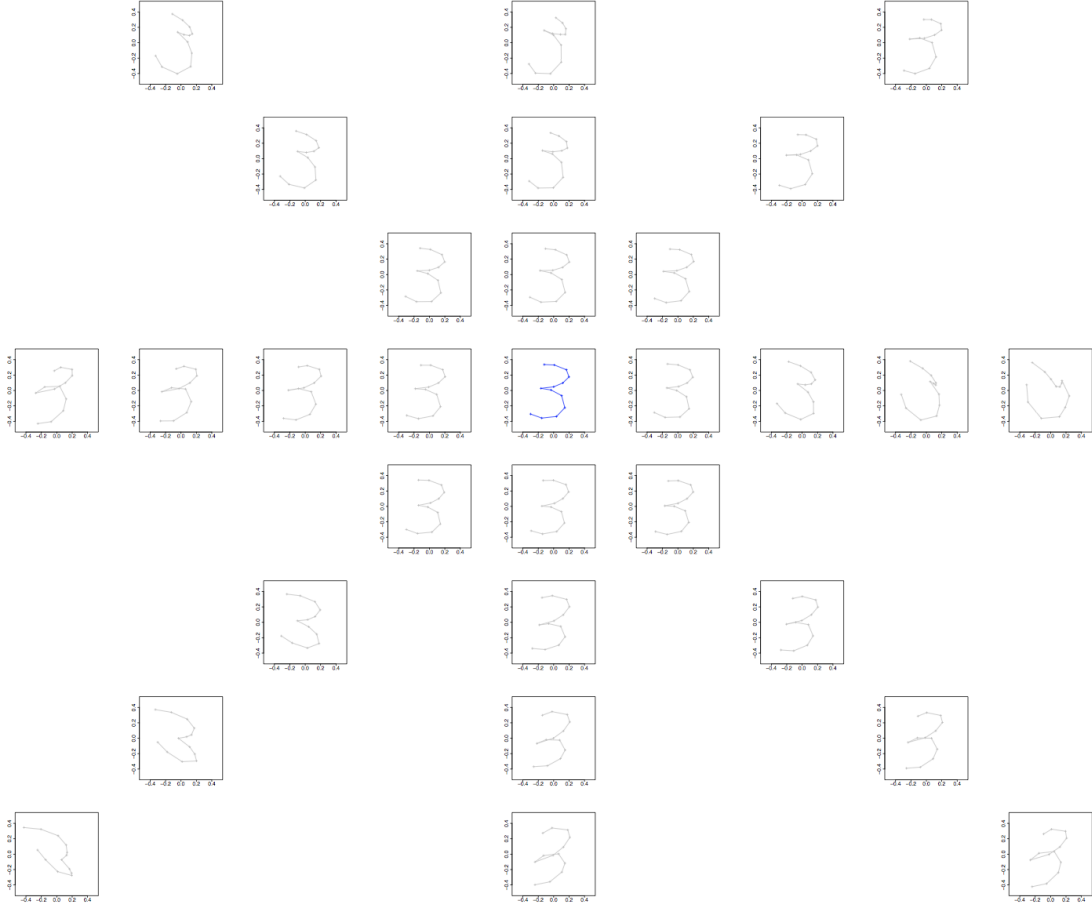


Figure 11: Principal sub-manifolds of the handwritten digits data, started from the center of symmetry. Among all the figures: the central figure (in blue) is the center of symmetry; the horizontal row contains images recovered from the first principal direction of the sub-manifold; the vertical column is the second principal direction; the main diagonal is the third principal direction; the other diagonal is the fourth principal direction.

generalization of many other statistical procedures. From the variance reduction perspective, one may think our proposed method as one of those competing methods that extend PCA on manifolds but not limited to only using lines or curves. This, potentially, can help us understand the data variation better and improve accuracy. From the classification point of view, this new method has been seen to be a useful tool to study shape changes. In the leaf growth example, we studied the only two main modes of shape variation. This has implied that one can extend a classification framework on the manifold. By projecting the new data points to any principal direction of the sub-manifold, one can calculate the distance and extend a classification rule based on all the distances. Surely, a successful classification also depends on 1) the data configuration; 2) how to define the local covariance matrix. If the data on the manifold is not too overlap, one might consider using a kernel density estimation. The label information needs also to be considered in the local covariance matrix, in which one would account for both of the between class and within class effects. As this is one of our on-going works, we will investigate it in the future.

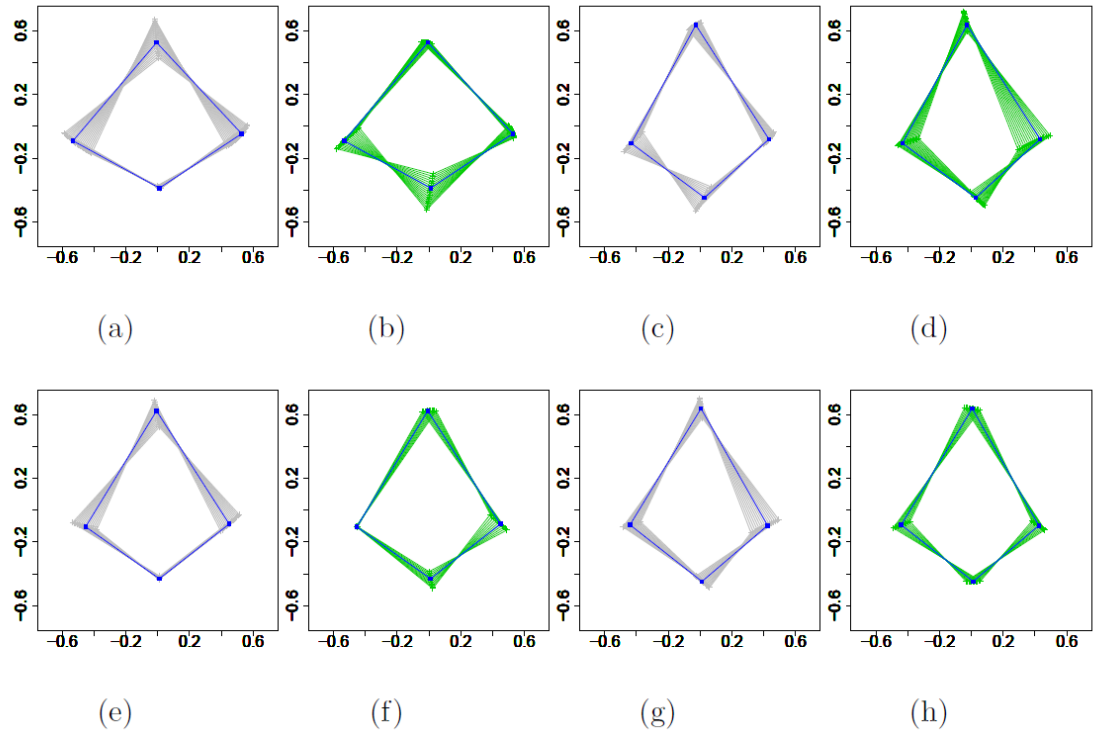


Figure 12: Principal sub-manifolds of the leaf growth data. (a) First principal direction obtained from the combined leaves at breast height and the crown of the reference tree; (b) Second principal direction obtained from the combined leaves at breast height and the crown of the reference tree. (c)-(h) provide the same information for clone 1, 2 and 3.

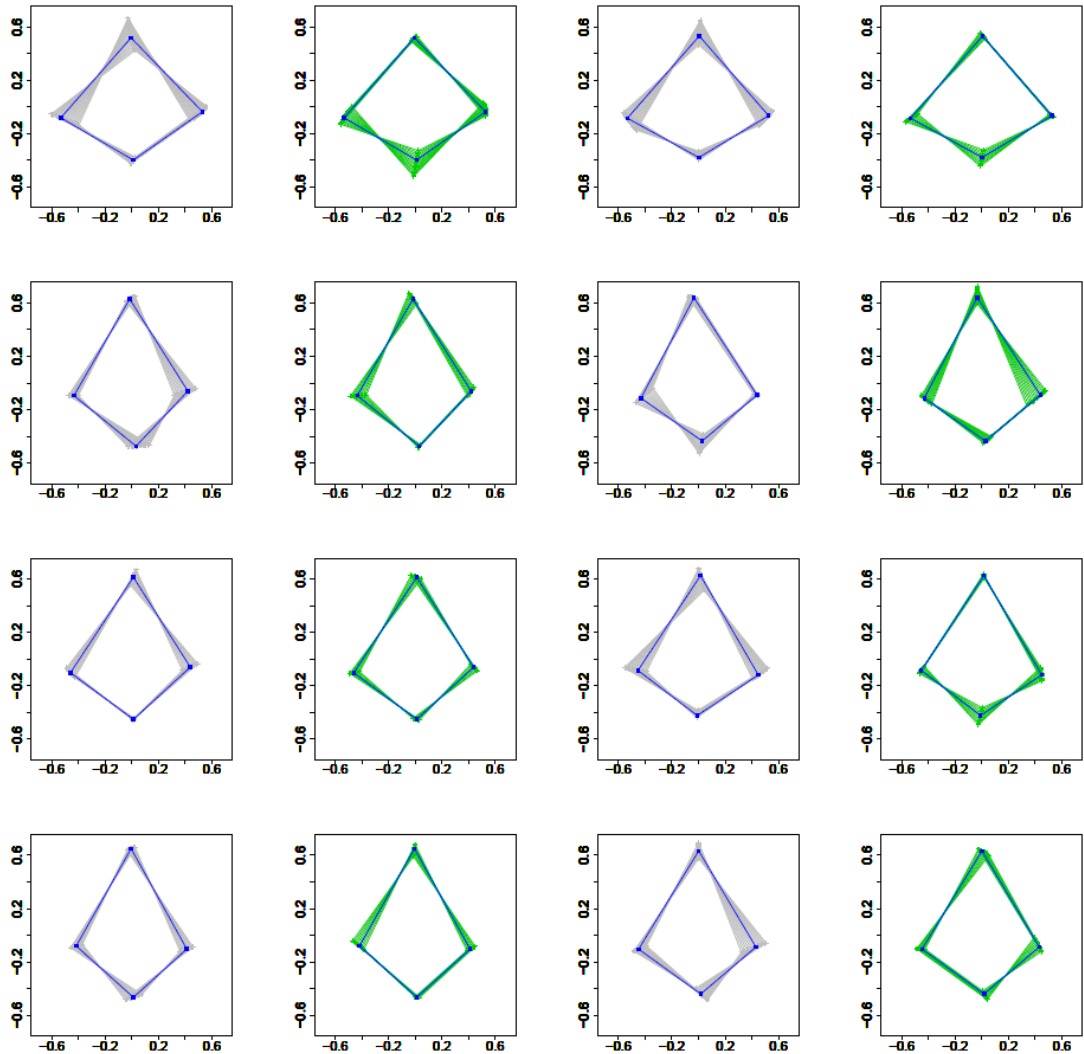


Figure 13: Principal sub-manifolds of the leaf growth data. Row 1 (reference tree): first principal direction at breast height; second principal direction at breast height; first principal direction at the crown; second principal direction at the crown. Row 2-Row 4 provide the same information for Clone 1, 2 and 3.

6 Proofs

Proofs of Formal Statements

6.1 Proof of Theorem 1

In the linear space \mathbb{R}^d ,

$$\Sigma_{B,\mathcal{M}} = \frac{1}{n} \sum_{i=1}^n (X_i - A)^\top (X_i - A) + (B - A)^\top (B - A).$$

By eigenvalue inequality,

$$\begin{aligned} \sum_{j=1}^k \lambda_j(B, \mathcal{M}) &\leq \sum_{j=1}^k \lambda_j(A, \mathcal{M}) + \text{trace}\left((B - A)^\top (B - A)\right) = \sum_{j=1}^k \lambda_j(A, \mathcal{M}) \\ &\quad + \|B - A\|^2. \end{aligned}$$

Let $D = \log_A(B)$, then

$$\|B - A\|^2 \leq \|D - A\|^2.$$

Putting all the results together,

$$\begin{aligned} \int_{D \in \log_A(\mathcal{N})} \left(\cos(\alpha_B) \times \sum_{j=1}^k \lambda_j(B, \mathcal{M}) \right) d\mu_k &\leq \int_{D \in \log_A(\mathcal{N})} \left(\sum_{j=1}^k \lambda_j(A, \mathcal{M}) + \|D - A\|^2 \right) d\mu_k \\ &= \int_{D \in \log_A(\mathcal{N})} \sum_{j=1}^k \lambda_j(D, \log_A(\mathcal{N})) d\mu_k. \end{aligned}$$

The inequality becomes equality when \mathcal{N} is a linear space spanned by $e_1(A, \mathcal{M}), e_2(A, \mathcal{M}), \dots, e_k(A, \mathcal{M})$.

References

- [1] Probal Chaudhuri and J. S. Marron. Scale space view of curve estimation. *The Annals of Statistics*, 28:408–428, 2000.
- [2] D. L. Donoho and C. Grimes. Hessian eigenmaps: New locally linear embedding techniques for high-dimensional data. *Proceedings of the National Academy of Sciences (PNAS)*, 102:7426–7431, 2003.
- [3] I. L. Dryden and K. V. Mardia. *Statistical Shape Analysis*. Wiley, New York, 1998.
- [4] R Fisher. Dispersion on a sphere. *Proceedings of the Royal Society A: Mathematical, Physical and Engineering Science*, 217:295–305, 1953.
- [5] P. T. Fletcher and S. Joshi. Riemannian geometry for the statistical analysis of diffusion tensor data. *Signal Processing*, 87:250–262, 2007.
- [6] P. T. Fletcher, C. Lu, S. M. Pizer, and S. Joshi. Principal geodesic analysis for the study of nonlinear statistics of shape. *IEEE Transactions on Medical Imaging*, 23:995–1005, 2004.

- [7] M. Fréchet. Les éléments aléatoires de nature quelconque dans un espace distancié. *Annales de l'Institut Henri Poincaré*, 10:215–310, 1948.
- [8] Samuel Gerber, Tolga Tasdizen, P. Thomas Fletcher, Sarang Joshi, Ross Whitaker, and the Alzheimers Disease Neuroimaging Initiative (ADNI). Manifold modeling for brain population analysis. *Medical Image Analysis*, 14:643–653, 2010.
- [9] T. Hastie and W. Stuetzle. Principal curves. *Journal of the American Statistical Association*, 84:502–516, 1989.
- [10] S. Huckemann, T. Hotz, and A. Munk. Intrinsic shape analysis: Geodesic pca for riemannian manifolds modulo isometric lie group actions. *Statistica Sinica*, 20:1–100, 2010.
- [11] S. Huckemann and H. Ziezold. Principal component analysis for riemannian manifolds, with an application to triangular shape spaces. *Advances in Applied Probability*, 38:299–319, 2006.
- [12] Stephan F. Huckemann. Intrinsic inference on the mean geodesic of planar shapes and tree discrimination by leaf growth. *The Annals of Statistics*, 39:1098–1124, 2011.
- [13] S. Jung, I. L. Dryden, and J. S. Marron. Analysis of principal nested spheres. *Biometrika*, 99:551–568, 2012.
- [14] Sungkyu Jung, Xiaoxiao Liu, J. S. Marron, and Stephen M. Pizer. *Generalized PCA via the backward stepwise approach in image analysis*, volume 83, chapter Advances in Intelligent and Soft Computing, pages 111–123. 2010.
- [15] P. E. Jupp and J. T. Kent. Fitting smooth paths to spherical data. *Journal of the Royal Statistical Society, Series C*, 36:34–36, 1987.
- [16] D. G. Kendall, D. Barden, T. K. Carne, and H. Le. *Shape and Shape Theory*. Wiley, New York, 1999.
- [17] K. Kenobi, I. L. Dryden, and H. Le. “shape curves and geodesic modelling. *Biometrika*, 97:567–584, 2010.
- [18] A. Kume, I. L. Dryden, and H. Le. Shape-space smoothing splines for planar landmark data. *Biometrika*, 94:513–528, 2007.
- [19] V. M. Panaretos, T. Pham, and Z. Yao. Principal flows. *Journal of the American Statistical Association*, 109:424–436, 2014.
- [20] X. Pennec and J.-P. Thirion. A framework for uncertainty and validation of 3d registration a framework for uncertainty and validation of 3d registration methods based on points and frames. *Int. Journal of Computer Vision*, 25:203–229, 1997.
- [21] Xavier Pennec. Intrinsic statistics on riemannian manifolds: Basic tools for geometric measurements. *Journal of Mathematical Imaging and Vision*, 25:127–154, 2006.